APSB
Acta Pharmaceutica Sinica B

ScienceDirect

Check for updates
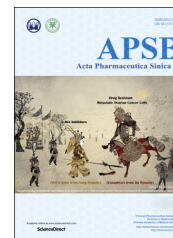
ORIGINAL ARTICLE

Updated developments on molecular imaging and therapeutic strategies directed against necrosis

Dongjian Zhang[a,b], Meng Gao[a,b], Qiaomei Jin[a,b], Yicheng Ni[a,b,c], Jian Zhang[a,b,*]

[a]*Affiliated Hospital of Integrated Traditional Chinese and Western Medicine, Nanjing University of Chinese Medicine, Nanjing 210028, China*
[b]*Laboratories of Translational Medicine, Jiangsu Province Academy of Traditional Chinese Medicine, Nanjing 210028, China*
[c]*Theragnostic Laboratory, Campus Gasthuisberg, KU Leuven, Leuven 3000, Belgium*

Abstract   Cell death plays important roles in living organisms and is a hallmark of numerous disorders such as cardiovascular diseases, sepsis and acute pancreatitis. Moreover, cell death also plays a pivotal role in the treatment of certain diseases, for example, cancer. Noninvasive visualization of cell death contributes to gained insight into diseases, development of individualized treatment plans, evaluation of treatment responses, and prediction of patient prognosis. On the other hand, cell death can also be targeted for the treatment of diseases. Although there are many ways for a cell to die, only apoptosis and necrosis have been extensively studied in terms of cell death related theranostics. This review mainly focuses on molecular imaging and therapeutic strategies directed against necrosis. Necrosis shares common morphological characteristics including the rupture of cell membrane integrity and release of cellular contents, which provide potential biomarkers for visualization of necrosis and necrosis targeted therapy. In the present review, we summarize the updated joint efforts to develop molecular imaging probes and therapeutic strategies targeting the biomarkers exposed by necrotic cells. Moreover, we also discuss the challenges in developing necrosis imaging probes and propose several biomarkers of necrosis that deserve to be explored in future imaging and therapy research.

1. Introduction

Cell death plays vital roles in living organisms and perturbations of cell death processes are an underlying factor of many pathological conditions. Excessive cell death is characteristic of acute myocardial infarction[1], sepsis[2], acute pancreatitis[3], and neurodegenerative disorders[4], among others. Cell death also plays a critical role in the treatment of certain diseases. Take cancer for example, most anticancer therapies, such as chemotherapy, radiation therapy and vascular-disrupting treatment, act by inducing the death of cancer cells[5–7]. With the growing knowledge of the mechanism of cell death, the classification of cell death modes has shifted from a traditional morphological to a biochemical classification[8]. In addition to the three canonical modes of cell death, namely apoptosis, necrosis and autophagy, other ways of dying such as necroptosis, pyroptosis and ferroptosis etc. have also been revealed[9,10]. Although there are many ways for a cell to die, only apoptosis and necrosis have been extensively studied in terms of cell death related molecular imaging and/or targeted therapy[11,12].

On one hand, noninvasive visualization and/or quantification of cell death contribute to gained insight into diseases, development of individualized treatment plans, evaluation of treatment responses, and prediction of patient prognosis. For instance, in the case of myocardial infarction (MI), the degree of apoptosis and necrosis can be significant and ascertaining the spatial and temporal occurrence of the two forms of cell death by molecular imaging can provide valuable diagnostic information on the risk stratification and therapeutic decision-making[13]. In the atherosclerosis case, lipid-rich necrotic core is a recognized feature of vulnerable atherosclerotic plaque[14] and its size is relevant to the risk of plaque rupture[15,16]. Assessing the size of lipid-rich necrotic core may help to provide prognostic information of atherosclerosis diseases and guide individualized treatment. In terms of cancer treatment, early assessment of tumor responses to therapy by cell death imaging should enable more effective patient management, allowing rapid selection of the most effective treatment, minimizing deleterious side effects from ineffective treatments and reducing health care costs.

On the other hand, cell death can also be targeted for the treatment of diseases. For example, tumor necrosis treatment (TNT) is such an approach to the treatment of solid tumors by targeting dead or degraded cells and a representative drug, iodine-131 labeled chimeric TNT (^{131}I-chTNT) monoclonal antibody (mAb) has been approved for clinical use in China[17]. Recently, another apoptosis-targeting medicine has also gained approval as a new class of anticancer agent called Venetoclax[18]. There are some other agents or strategies targeting cell death are under active development or exploration[19–21].

Apoptosis imaging/targeted therapy has been extensively described in other reviews[22,23], and therefore is not within the scope of this review. In the present review, we summarize the updated joint efforts to develop molecular imaging probes and therapeutic strategies through targeting the biomarkers exposed by necrotic cells. We also discuss the challenges in developing necrosis imaging probes and propose several biomarkers of necrosis that deserve to be explored in future imaging and therapy research.

2. Necrosis and its biomarkers

Necrosis is the consequence of irreversible damage to cells that results from acute physicochemical injuries or sudden metabolic failures such as mechanical trauma, infections, toxins and ischemia. Necrosis has long been considered as an accidental and unregulated form of cell death. It has often been contrasted to apoptosis, which is a highly regulated and genetically defined cellular process as a result of response to internal (mitochondrial disruption) or external (death-domain receptor activation) stimuli. Recently, there are increasing evidences that necrosis can also occur in a regulated modality under certain circumstances[9,10]. Moreover, in some cases, a dying cell can even switch between different programs of cell death, for example, apoptotic cells may suffer from (secondary) necrosis in conditions of insufficient phagocytosis. Although the subroutines of cell death are diverse, necrosis shares common morphological characteristics including the rupture of cell membrane integrity and the release of cellular contents, thus triggering inflammation in the surrounding cell milieu[24]. While apoptosis is the atrophy of a cell that maintains the integrity of the cell membrane, and the biggest characteristic of this type of cell death is its ability to limit the overproduction of inflammatory reactions. Therefore, the loss of cell membrane integrity is the most important feature to distinguish necrosis from apoptosis.

Contents released by necrotic cells provide potential biomarkers for visualization of necrosis and necrosis targeted therapy. The biomarkers that have been targeted for necrosis imaging and/or targeted therapy[11,12,25–28] including DNA/histone H1 complex, exposed DNA, heat shock protein 90 (Hsp90), lupus-associated (La) antigen, histones, high mobility group box 1 (HMGB1), fumarase and other unknown molecules (Table 1). To achieve accurate visualization of necrosis, the specificity of targeted biomarkers is critical. Among these biomarkers above, DNA/histone H1 complex, exposed DNA, Hsp90 and fumarase are specific to necrotic or damaged cells that lose their plasma membrane integrity. While La antigen, histones and HMGB1 are not completely specific to necrosis. Take La antigen and histones for instance, apart from that exposed in cases of necrosis, they can also be exposed when apoptosis occurs[115,116]. For HMGB1, except for the passive release from necrotic or damaged cells, it can also be actively secreted by cells under severe stress or by stimulated immune cells in response to various exogenous or endogenous stimuli[31]. Therefore, when these less specific biomarkers are used for imaging necrosis, the possible overestimation of the extent of necrosis should be kept in mind.

3. Molecular imaging and therapeutic strategies targeting necrosis biomarkers

It has been three decades since necrosis was utilized as a target for diagnosis and treatment of diseases[118–120]. In this section, we will describe the recent developments on molecular imaging and therapeutic strategies targeting necrosis biomarkers.

3.1. DNA/histone H1 complex

TNT is an innovative approach to cancer imaging and therapy utilizing necrotic tissue as a target for the selective binding of mAbs[118]. The first TNT mAb, designated TNT-1, was directed against common intracellular antigen DNA/histone H1 complex, which was exposed in the necrotic core of solid malignancies[121,122]. However, preclinical animal studies showed that biodistribution of TNT-1 to human xenografts was similar to other antibodies against solid tumors—about 2% of an injected dose per gram tumor tissue[123]. Therefore, it is desirable to augment its uptake in the tumor while minimize non-specific binding in normal

Table 1 Overview of imaging and therapeutic studies targeting necrosis biomarkers.

Biomarker	Targeting moiety	Imaging modality	Therapeutic application	Ref.
DNA/histone H1 complex	chTNT-1/B	SPECT	Solid tumors	19,29–31
	NHS76	SPECT, PET,	Solid tumors	32–38
Exposed DNA	chTNT-3	SPECT, PET, Immunoscinti-graphy	Solid tumors	17,39–46
	TO-PRO-1	MRI	–	47,48
	Hoechst 33258	FLI, SPECT	HT29 colon tumor, HCT-116 tumor, MI	49–53
	Hyp	SPECT, PET	Rhabdomyosarcoma, RIF-1 tumor, H22 tumor, S180 tumor, VX2 tumor, W256 tumor	54–66
	HDA	SPECT	–	67
	Shyp	SPECT	–	68
	Hypomycin A	SPECT	–	69
	Rhein	SPECT	–	70,71
	1-hydroxyantha-quinone	PET	–	72
	Naphthazarin	SPECT	–	73
	Vitexin	SPECT	–	74
Hsp90	GSAO	FLI, SPECT	–	75–79
La antigen	DAB4	γ-Scintigraphy	Lewis Lung carcinoma, EL4 lymphoma, LNCaP tumor, Panc-1 tumor	80–83
Histones	Glucarate	SPECT	–	84
	Heparin	–	Lethal thrombosis	85–87
	Chondroitin sulfate	–	Lethal thrombosis	87
	BWA-3	–	Sepsis, acute organ injury	88–90
HMGB1	2G7	–	Arthritis, sepsis, neuropathic pain, acetaminophen (APAP)-induced liver injury, pancreatitis and pancreatic islet graft transplantation	91,92
	h2G7	–	APAP-induced liver injury	93,94
	Glycyrrhizin	–	Ischemia/reperfusion -induced spinal cord, liver, brain and myocard injury, sepsis, cancer	91,92,95
	Carbenoxolone	–	Peptic ulceration, inflammation	91,95
	Salicylic acid	–	Mesothelioma	91,92
	Metformin	–	APAP-induced acute liver injury	96
Fumarase	Hyperpolarized [1,4-$^{13}C_2$]fumarate	13C MRS, 13C MRI	–	97–101
Unknown	Protohypericin	SPECT	A549 tumor	102,103
	Sennidin A	SPECT	S180 tumor	104,105
	Sennoside B	SPECT	–	106,107
	Sennidin B	SPECT	–	107
	Skyrin	SPECT	–	108
	HQ5	FLI, MSOT	–	27
	IRDye800CW	FLI, MRI	–	27,109
	HQ4	FLI, SPECT, MSOT	–	110,111
	ICG	FLI	–	28,112
	EB	MRI	–	113,114

–Not reported.

tissues. Khawli et al.[124] found that biotinylated chimeric TNT-1 (chTNT-1/B) not only had faster whole body clearance and better biodistribution profiles but also showed enhanced tumor uptake compared with non-biotinylated parent antibody. Iodine-131 labeled chTNT-1/B (^{131}I-chTNT-1/B) had been evaluated in Phases I and II trials for treatment of patients with malignant gliomas administered *via* convection-enhanced delivery[19,29–31]. Although safe and tolerable dosing regimens had been identified, further clinical experience is needed to assess its efficacy for treatment of malignant gliomas[19,31]. Moreover, a fully human mAb, designated NHS76, had been developed with similar binding characteristics to chimeric TNT-1 (chTNT-1)[125] and showed

potential for tumor immunotherapy by selectively delivering bioactive molecules to the necrotic regions of solid tumors[32–38].

3.2. Exposed DNA

Exposed DNA is a common biomarker for necrosis, which is normally located in cell nucleus and becomes exposed after loss of cell plasma membrane integrity. A number of molecular probes and several therapeutic strategies have been developed to target exposed DNA for imaging of necrosis and treatment of necrosis-related diseases. The chimeric TNT-3 (chTNT-3) mAb, which is

directed against exposed single-stranded DNA, had been developed and compared the potential for diagnostic imaging with a series of its derivatives after being labeled with different radionuclides[39–41,126]. However, no recent developments about imaging applications have been reported except that a micro-positron emission tomography/computed tomography (PET/CT) imaging studies of copper-64 labeled chTNT-3 in MAD109-bearing mice was used to demonstrate clinical relevancy of using chemotherapy pretreatment to increase necrosis-targeting antibody uptake[42]. In terms of therapeutic applications, ^{131}I-chTNT mAb had been approved for the treatment of advanced lung cancer in China, making it the first approved radiolabeled antibody for the treatment of solid tumors worldwide[17]. Considering that the more necrosis, the more anchorage for the TNT antibodies. The combination of ^{131}I-chTNT mAb with necrosis-inducing procedures, for example, radiofrequency ablation, had been explored and demonstrated enhanced tumor accumulation of this radiopharmaceutical and superior efficacy to radiofrequency ablation alone for treatment of middle-advanced stage hepatocellular carcinoma in short-term follow-up[43,127]. Moreover, chTNT-3 had also been utilized to selectively deliver other therapeutic molecules for the treatment of solid tumors[44–46].

In addition to the antibody molecules described above, small molecular compounds have also been actively explored for necrosis imaging and/or targeted therapy. Gd-TO (Fig. 1), a TO-PRO-1-based gadolinium labeled probe, which binds to DNA through electrostatic interactions[47], could visualize not only acute necrosis but also the clearance of necrotic debris from the infarcted myocardium in mouse models of MI by magnetic resonance imaging (MRI)[48]. Hoechst-IR (Fig. 1), consisting of a near-infrared dye IR-786 conjugated to a DNA binding agent Hoechst 33258, allowed visualization of necrotic tissues in mouse models with MI or sepsis by fluorescence imaging (FLI)[49]. In the follow-up studies, H-gemcitabine and H-IGF1 were designed for selectively delivering gemcitabine and IGF-1 to the necrotic core of tumors and the infarcted myocardium, respectively, to reduce the systemic toxicity of gemcitabine and protect from cardiac fibrosis and dysfunction following MI[50,51]. Furthermore, Hoechst 33258-conjugated hyaluronated fullerene was designed to target exposed DNA present in the necrotic tumor and could cause significantly increased tumor inhibition in multiple photodynamic therapies[52]. The above favorable results motivated us to construct a Hoechst 33258-based radioactive tracer for early evaluation of tumor response to treatment of vascular-disrupting agents. The results suggested that iodine-131 labeled Hoechst 33258 could visualize tumor necrosis induced by combretastatin A-4 disodium phosphate (CA4P) via single photon emission computed tomography/computed tomography (SPECT/CT) imaging in W256 tumor-bearing rats[53].

Initially, hypericin (Hyp), a naturally occurring naphthodianthrone compound found in Hypericum perforatum[128], was demonstrated to have extraordinary necrosis avidity and showed diagnostic potential for MI after being labeled with iodine-123 (Fig. 1)[54–56]. However, images of good diagnostic quality could not be obtained until 9 h post injection (p.i.) due to high blood pool activity[54]. Moreover, the high uptake in mononuclear phagocyte system (MPS), resulting from the formation of aggregates[129], can interfere with the imaging of necrotic myocardium. Therefore, in order to improve the speed and quality of imaging, enhancing blood clearance and reducing unwanted biodistribution in MPS is desirable. It was reported that introduction of hydrophilic group(s) into a molecule moiety could improve the hydrophilicity, thus drastically decreasing or even preventing the aggregation of molecules and improving the pharmacokinetics[130–133].

Based on the above enlightenment, iodine-131 labeled hypericin dicarboxylic acid (^{131}I-HDA) (Fig. 1) and the more water-soluble iodine-131 labeled hypericin-2,5-disulfonic acid sodium salts (^{131}I-Shyp) (Fig. 1) were synthesized and evaluated for their potential to rapidly visualize necrotic myocardium[67,78]. The results revealed that clear visualization of necrotic myocardium was achieved at 6 h p.i. of ^{131}I-HDA and 4 h p.i. of ^{131}I-Shyp by SPECT/CT imaging in rat models with MI (Fig. 2), both earlier than that of iodine-131 labeled Hyp (^{131}I-Hyp)[67,68]. This suggested that introduction of hydrophilic groups into a probe entity was a feasible strategy to improve its pharmacokinetic and biodistribution characteristics. The in vitro DNA binding studies and in vivo blocking experiments suggested that the necrosis avidity mechanism of Shyp and Hyp might be attributable to the intercalation with exposed DNA[67,68]. Considering that HDA and Hyp have the same target of necrotic tissues[67], we conclude that the necrosis avidity mechanism of HDA may also be due to the intercalation with exposed DNA.

On the other hand, twisting the aromatic core or reducing the size of π-core will make the formation of aggregates more difficult[130,134]. With this in mind, we determined the aggregation constants of four natural hypocrellins, which possess less π-conjugated cores and more distorted structures compared with Hyp. The results showed that the aggregation capability of hypocrellins was much lower than that of Hyp[69]. After labeled with iodine-131, necrosis avidity of the four tracers was evaluated, and ^{131}I-hypomycin A emerged as the most promising one[69]. SPECT/CT imaging showed that necrotic myocardium could be visualized at 4 h p.i. of ^{131}I-hypomycin A in rat models of MI, earlier than that of ^{131}I-Hyp[69]. Moreover, preliminary mechanism studies suggested that the necrosis avidity of ^{131}I-hypomycin A might be due to its binding to the exposed DNA in necrotic tissues[69].

Although significant progress has been made, our efforts go beyond that. We also explored the necrosis avidity of anthraquinones, which hold more simplified structures and are a class of typical DNA intercalating agents[135]. Eight radioiodinated monomeric anthraquinones were manifested to have avidity to necrotic tissues and iodine-131 labeled rhein (Fig. 1) emerged as the most promising one[70]. Necrotic myocardium could be clearly visualized by SPECT/CT imaging at 6 h p.i. in rat models of MI (Fig. 3)[70]. In order to develop a probe suitable for clinical diagnosis, we subsequently synthetized three technetium-99m labeled rhein derivatives and found that the necrotic myocardium lesion could be clearly visualized by SPECT/CT imaging at 1 h p.i. of [99m]Tc(EDDA)-HYNIC-2C-rhein (Fig. 1) in rat models of MI (Fig. 4B)[71]. Furthermore, three fluorine-18 labeled 1-hydroxyanthraquinone derivatives were also synthesized and evaluated for their potential to rapidly image necrotic myocardium. Among them, [^{18}F]FA3OP (Fig. 1) emerged as the most promising one and allowed rapid visualization of necrotic myocardium by PET/CT imaging at 1 h p.i. in rat models of MI (Fig. 4A)[72]. The in vitro DNA binding studies and in vivo blocking experiments suggested that the necrosis avidity mechanism of [99m]Tc(EDDA)-HYNIC-2C-rhein and [^{18}F]FA3OP might be attributable to their interaction with exposed DNA in necrotic tissues[71,72].

Considering that 1,4-naphthoquinones may achieve faster imaging of necrotic myocardium as they hold enhanced blood clearance relative to anthraquinones, we evaluated the necrosis avidity of radioiodinated 1,4-naphthoquinones and their potential for rapidly visualizing necrotic myocardium. The results showed that six radioiodinated 1,4-naphthoquinones still retained necrosis avidity and iodine-131 labeled naphthazarin (^{131}I-naphthazarin) (Fig. 1) could visualize necrotic myocardium at 3 h p.i. when it
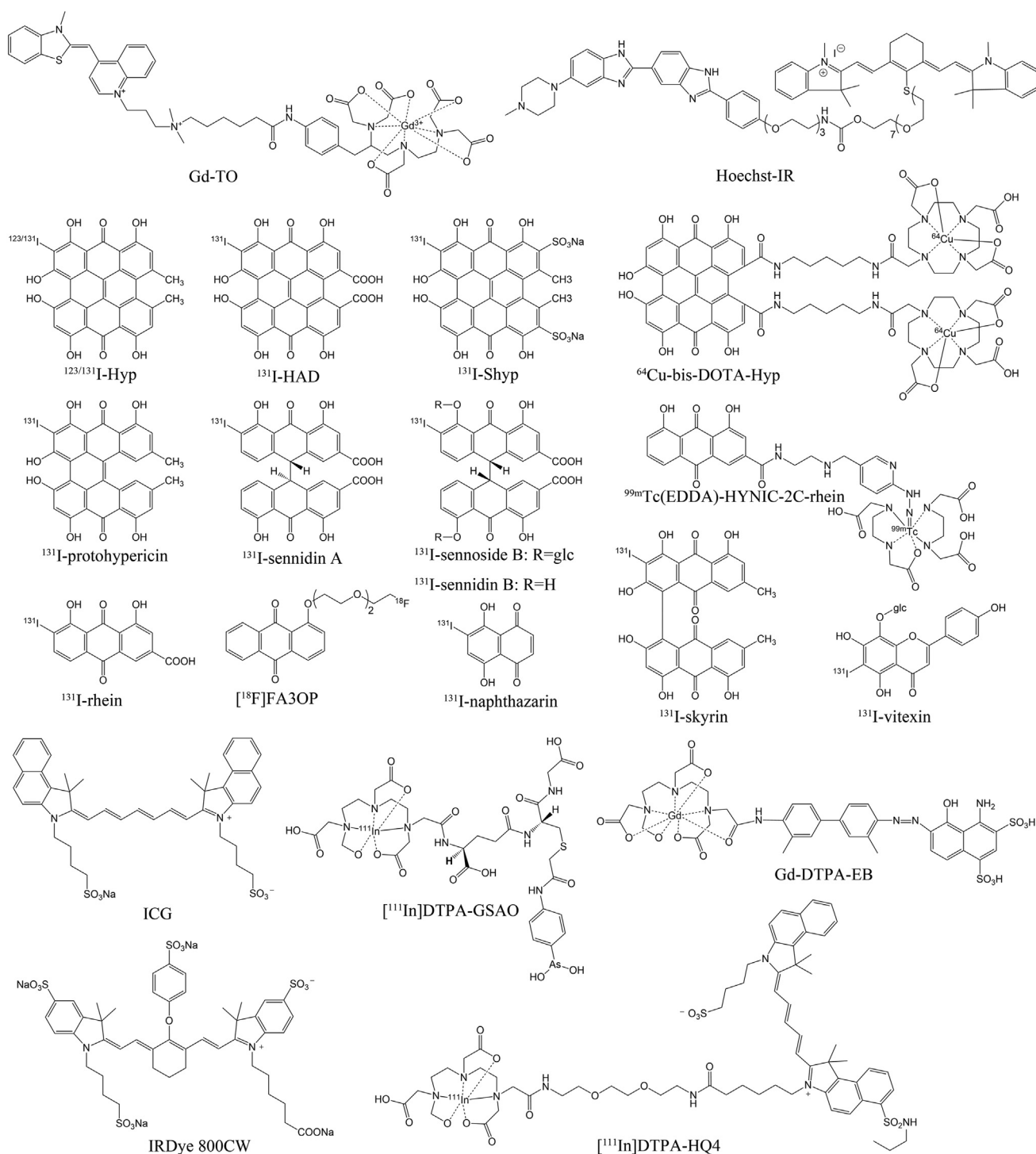
Figure 1 Chemical structures of some representative small molecule probes targeting necrosis.

was impossible for ^{131}I-rhein[73]. Seeing that naphthazarin still retained the planar aromatic structure[136], we explored its ability to bind to DNA. The results demonstrated that naphthazarin had a moderate bind affinity to DNA *in vitro*[73]. Combination with *in vivo* blocking experiments suggested that the necrosis avidity mechanism of ^{131}I-naphthazarin may be due to its binding to exposed DNA present in necrotic tissues. Future imaging research involves labeling with more appropriate radionuclides such as

iodine-123, technetium-99m or fluorine-18, which may provide better imaging quality and faster imaging.

Except for quinone compounds described above, we recently evaluated the necrosis avidity of flavonoids, which are a class of safe naturally available polyphenolic compounds and reported to be able to bind to double-stranded DNA mainly through intercalation[137]. Among eight radioiodinated 5,7-dihydroxyflavones, iodine-131 labeled vitexin (^{131}I-vitexin) (Fig. 1) emerged as a lead
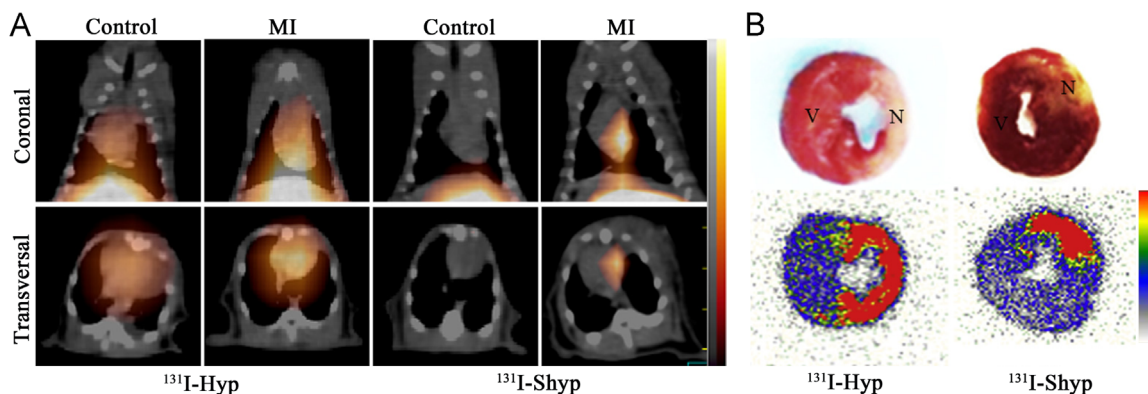
Figure 2 (A) Coronal and transversal SPECT/CT images obtained at 4 h post injection of ^{131}I-Shyp or ^{131}I-Hyp in rats with reperfused myocardium infarction (MI) or sham operation. (B) TTC staining images (upper panels) and corresponding autoradiographs (under panels) of myocardial sections from rats with MI. Necrotic myocardial areas showed pale, while viable myocardial areas were stained brick red. N, necrotic area; V, viable area (Adapted from Ref. 68 with permission. Copyright © 2017 Elsevier).
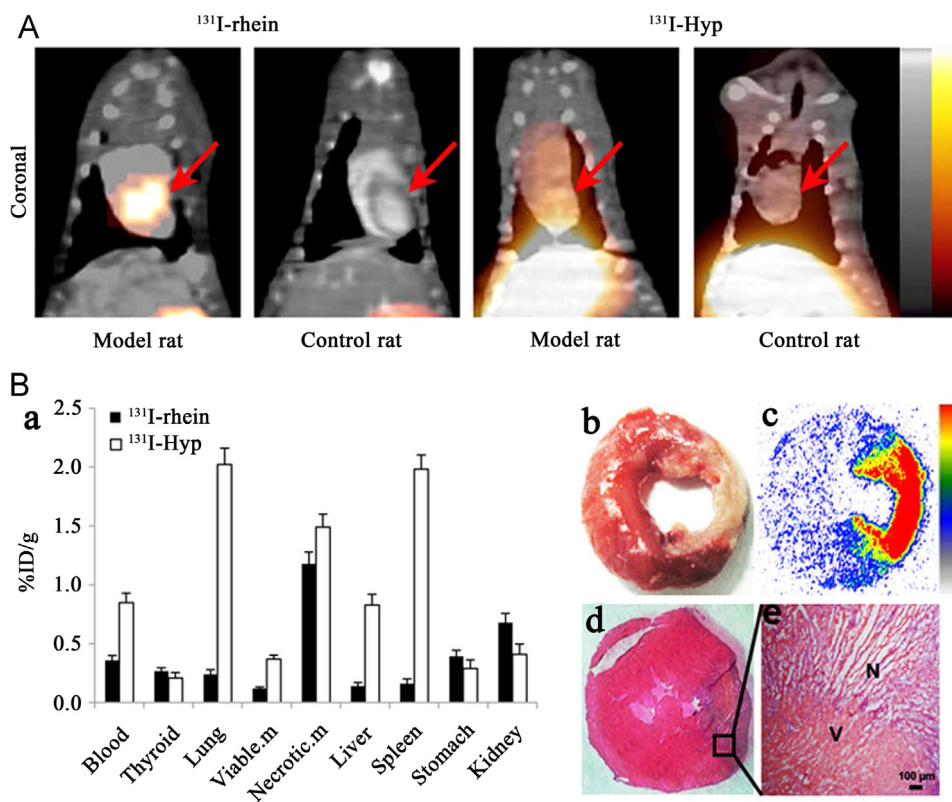

Figure 3 (A) Representative coronal SPECT/CT images of rats with reperfused myocardium infarction or sham operation obtained at 6 h post injection of ^{131}I-rhein or ^{131}I-Hyp. Red arrows indicate the heart. (B) Postmortem verification in model rats after SPECT/CT imaging. (a) Biodistribution of ^{131}I-rhein and ^{131}I-Hyp at 6 h post injection ($n = 5$ for each tracer). %ID/g represents the percentage of injected dose per gram of tissue. Data are mean ± standard deviation. Viable. m, viable myocardium; Necrotic. M, necrotic myocardium. (b)–(e) Postmortem analysis of myocardial slices from model rats receiving ^{131}I-rhein: (b) TTC staining image of 2 mm thick slice; (c) autoradiograph of 50 μm frozen section; (d) H&E staining image of 10 μm frozen section; (e) H&E staining microphotograph, proving the presence of necrosis. N, necrotic area, V, viable area (Adapted with permission from Ref. 70. https://creativecommons.org/licenses/by/4.0/).

tracer and could image tumor necrosis induced by CA4P treatment *via* SPECT/CT imaging at 4 h p.i. in W256 tumor-bearing rats (Fig. 5)[74]. The *in vitro* DNA binding studies and *in vivo* blocking experiments suggested that the necrosis avidity mechanism of ^{131}I-vitexin may be due to its interaction with exposed DNA in necrotic tissues[74].

3.3. Hsp90

The Hsp90 plays a critical role in a number of fundamental cellular processes by involving in the folding, stabilization, activation and assembly of a variety of "client" proteins[138]. Hsp90 is the most abundant molecular chaperone of the eukaryotic cytoplasm,
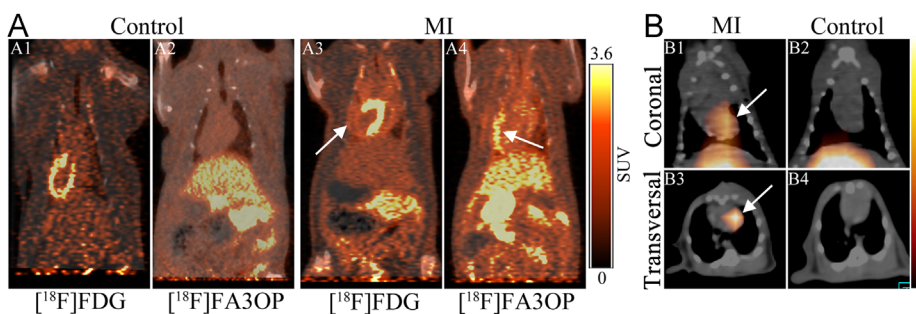
Figure 4 (A) Representative coronal PET/CT images of control rats and model rats with reperfused myocardium infarction (MI) at 1 h after administration of [^{18}F]FDG (A1, A3) and [^{18}F]FA3OP (A2, A4). White arrows indicate the location of necrotic myocardium. (B) Representative coronal (B1, B2) and transversal (B3, B4) SPECT/CT images of rats with reperfused MI or sham operation at 1 h after injection of ^{99m}Tc(EDDA)-HYNIC-2C-rhein. White arrows indicate the heart. (Adapted with permission from Refs. 71 and 72. Copyright © 2017 American Chemical Society).
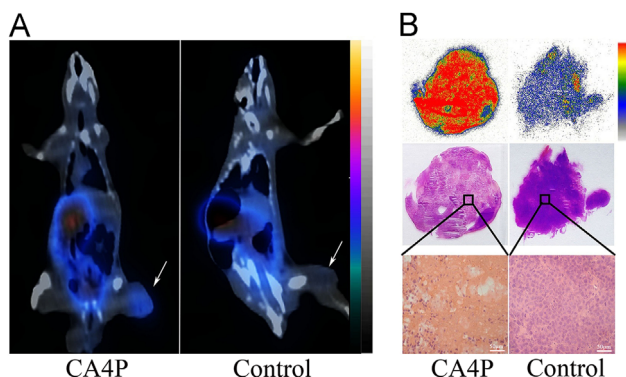

Figure 5 (A) Representative coronal SPECT/CT images of W256 tumor-bearing rats obtained at 4 h post injection of ^{131}I-vitexin. W256 tumor-bearing rats were pretreated with 20 mg/kg combretastatin A-4 disodium phosphate (CA4P) or were left untreated (Control) for 24 h. White arrows indicate significantly different uptakes of the tracer in the tumors of model and control rats. (B) Autoradiographs, corresponding H&E staining images and micrographs of 10 μm tumor slices from model and control rats administered with ^{131}I-vitexin. (Adapted with permission from Ref. 74. Copyright © 2018 American Chemical Society).

comprising 1%–2% of the intracellular protein contents in unstressed cells and increasing to 4%–6% of cellular proteins under stress[139]. It had been targeted by a small organoarsenical compound, 4-(N-(S-glutathionylacetyl)amino)phenylarsonous acid (GSAO) labeled with fluorophores and radionuclides (Fig. 1) for imaging of cell death in animal models of tumors, traumatic brain injury, and myocardial infarction or ischemia[75–78]. GSAO is a peptide trivalent arsenical that rapidly accumulates in the cytoplasm of dying and dead cells coincident with loss of plasma membrane integrity. It is retained in the cytosol predominantly through covalent reaction with the Cys597, Cys598 dithiol of Hsp90 by its As(III) atom, forming a stable cyclic dithioarsinite[79,140]. As very few appropriately spaced cysteine thiols exist in the extracellular milieu, GSAO is largely unreactive until it crosses the plasma membrane. GSAO cannot reach its intracellular target molecules in viable or early-stage apoptotic cells, because it cannot cross the intact plasma membrane. For necrotic cells, the plasma membrane integrity is completely disrupted, which allows free access of GSAO to the cell interior. Therefore, when tagged with optical or radioactive reporter groups, GSAO can selectively label dead cells with loss of plasma membrane integrity.

3.4. La antigen

The La antigen is an abundant, essential and ubiquitously expressed ribonucleoprotein, which is an RNA-binding chaperone primarily localized to the nucleus although it may shuttle to cytoplasm[141]. La is revealed preferentially in dead tumor cells and is cross-linked by transglutaminase 2[80,142], thus stabilizing the antigen. The loss of cell membrane integrity makes intracellular La accessible to bind by specific monoclonal antibody[142]. Therefore, La represents a promising dead cancer cell target for imaging treatment response as well as tumor radioimmunotherapy.

The La-specific monoclonal antibody, DAB4 (also known as APOMAB®) was demonstrated to be able to specifically target dead tumor cells in vivo[143], and targetability was augmented after DNA-damaging treatment[81,82,143,144]. A recent study further demonstrated the selectivity of DAB4 for chemotherapy-induced dead tumor cells and this postchemotherapy selectivity was related to a relative increase in the availability of DAB4-binding targets in tumor tissue rather than in normal tissues[115], which provided further evidence to support the diagnostic use of DAB4 as a predictive marker of treatment responses. On the other hand, DAB4 radiolabeled with Lu-177 and Th-227 had been exploited for tumor therapy, with supra-additive responses observed when combined with chemotherapy[80,83]. A Monte Carlo simulations study suggested that the dose distribution resulting from Pb-212 was more suitable for tumor necrosis targeted alpha therapy than that from a pure β-emitter, which may provide a solution to the problem of treating hypoxic tumor cells resistant to conventional external beam radiotherapy[145].

3.5. Histones

Histones are highly conserved, intra-nuclear cationic proteins that are normally organized into nucleosomes (H2A, H2B, H3 and H4) or located on the internucleosomal DNA (H1 and H5) in all eukaryotic cells. It can be passively released into the extracellular space during necrosis, which occurs extensively in various pathologies[146–148]. Once released into the extracellular milieu, histones function as damage associated molecular pattern (DAMP) molecules, leading to significant proinflammatory and toxic responses[88,89,149–151]. Therefore, extracellular histones may serve as useful biomarkers for the diagnosis and treatment of related pathologies.

Glucarate is a natural catabolite of D-glucuronic acid in mammals. Technetium-99m labeled glucarate (^{99m}Tc-glucarate) was initially described as a tracer accumulating in MI and zones of cerebral injury[152,153]. Later ^{99m}Tc-glucarate was demonstrated to be also able to distinguish necrotic cells from apoptotic cells in leukemic tumor cell line U937[154]. The specificity of ^{99m}Tc-glucarate for necrosis is likely due to that the loss of membrane integrity allows entry and intracellular diffusion of ^{99m}Tc-glucarate where its negative charge attracts and binds to the positively charged histones[155]. More recently, ^{99m}Tc-glucarate has been used for *in vivo* quantification and visualization of necrotic area and therapeutic effect of paclitaxel in ovarian cancer xenografted nude mice and demonstrated to be an effective radiotracer for evaluation and monitoring of tumor necrosis caused by chemotherapy[84].

Moreover, extracellular histones provide potential target for the treatment of certain diseases as they play vital pathological roles in tissue injury and inflammatory diseases[146–148]. An initial proof-of-principle study indicated that antibody to histone H4 (BWA-3) could reduce the mortality of mice in lipopolysaccharide, tumor necrosis factor or cecal ligation and puncture models of sepsis[88]. Thereafter the protective effects of anti-histone mAbs were further corroborated in animal models of acute organ injury[90,147,156–158]. The results are encouraging and pave the way for future development of drugs with similar pharmacodynamic properties for human use. Recently, two clinically used mucopolysaccharide compounds, heparin and chondroitin sulfate, have been demonstrated to show strong bind to histones and be able to neutralize extracellular histone-mediated cytotoxicity[85–87]. Although these histone-neutralizing therapeutic strategies have proven to provide significant protection from mortality in animal models of acute organ injury or sepsis, further research is requisite to warrant their safe application in clinical settings[148]. Moreover, what interests us is that apart from their therapeutic role by neutralizing extracellular histones, heparin and chondroitin sulfate may act as effective molecular scaffolds for developing necrosis imaging probes.

3.6. HMGB1

HMGB1 is a non-histone chromosomal protein that plays a pivotal role not only inside of the cell as a DNA chaperone, chromosome guardian, autophagy sustainer, and protector from apoptotic cell death, but also outside the cell as a DAMP molecule[117]. HMGB1 is passively released from cell nucleus into the extracellular milieu during necrosis[159–161]. Released HMGB1 can interact with a number of pattern recognition receptors and mediate a broad range of pathological responses[162–168]. These characteristics make extracellular HMGB1 a critical molecular target for the treatment of multiple diseases including inflammatory diseases, stroke, ischemia reperfusion injury, immune disorders, metabolic disorders, pancreatic diseases and cancer[91–93,169,170].

A number of therapeutic strategies have been proposed to directly target HMGB1 or HMGB1-receptor signaling pathway. Current pharmacological strategies include the use of anti-HMGB1 antibodies, peptide and protein, soluble receptors, microRNAs, and small molecules[91,92,94–96]. Although HMGB1-targeting therapeutic strategies have been extensively evaluated in many experimental models, there has not been a study targeting HMGB1 for molecular imaging, which may help in detection or diagnosis of HMGB1-related pathologies and prediction of response to therapeutic interventions. As a generic strategy, it may be feasible to develop molecular probes based on anti-HMGB1 antibodies

(*e.g.*, 2G7[91,92], h2G7[93,94]) or small molecule compounds directly binding to HMGB1 (*e.g.*, glycyrrhizin[91,92,95], carbenoxolone[91,95], salicylic acid[91,92] and metformin[96]) for visualization of necrosis.

3.7. Fumarase

Fumarate is a tricarboxylic acid cycle intermediate, which is hydrated to produce malate catalyzed by the intracellular enzyme fumarase. Unlike many metabolic reactions, the fumarase reaction requires no coenzymes or cosubstrates (other than water) and still retains activity even during cell death[97]. Gallagher et al.[97] found that [1,4-^{13}C$_2$]malate production from [1,4-^{13}C$_2$]fumarate was increased in treated lymphoma cells and tumors, and that this increase was caused by necrosis of tumor cells, which makes the conversion of [1,4-^{13}C$_2$]fumarate to [1,4-^{13}C$_2$]malate suitable as a sensitive marker of cell necrosis and treatment response in tumors. The subsequent studies showed that the production of [1,4-^{13}C$_2$] malate from hyperpolarized [1,4-^{13}C$_2$]fumarate could offer positive magnetic resonance contrast to identify cellular necrosis in implanted tumors, acute kidney injury and MI[98–100]. Another study demonstrated that magnetic resonance spectroscopy of co-polarized ^{13}C-labeled pyruvic acid and ^{13}C-labeled fumaric acid could non-invasively detect both necrosis and lactate efflux in tumor cells[101]. These data, together with the ongoing clinical trials of hyperpolarized ^{13}C MRI[171,172], supported that hyperpolarized [1,4-^{13}C$_2$]fumarate MRI could offer an alternative noninvasive method in the clinic to detect the early response of tumors to treatment, identify a window of therapeutic opportunity for patients, and measure cellular necrosis in heart diseases.

3.8. Other unknown targets

There are some other molecular probes or radioactive agents that show high avidity to necrotic tissues but their mechanisms are still not well-known. Here, we still have to start with Hyp. Apart from its potential for imaging necrotic myocardium after labeled with iodine-123[54–56], Hyp had also been extensively explored for the treatment of diverse solid tumors or evaluation of therapeutic efficacy after labeled with iodine-131 or copper-64 (Fig. 1)[57–65]. Despite the substantial translational potential related to certain oncological and non-oncological applications[66], some inherent defects such as extremely poor water solubility, easy to form aggregates and deep colors may haunt its further clinical transformation. Except that the formulation approach had been used to solubilize Hyp[173–175], structural modifications had also been attempted to solve the problems confronted. It was reported that the distortion of the π systems or reducing the size of π-conjugated core not only could improve aqueous solubility of molecules[176,177], but also could decrease or even prevent the aggregation of molecules[130,134]. As an initial attempt, protohypericin was synthetized and evaluated aiming at searching for novel necrosis avid compound with less self-aggregation ability relative to Hyp by reducing the size of π-conjugated core[102]. The results showed that iodine-131 labeled protohypericin (^{131}I-protohypericin) (Fig. 1) still retained necrosis avidity and presented a weaker aggregation ability compared with ^{131}I-Hyp[102]. Combined treatment using ^{131}I-protohypericin and CA4P could prolong the survival of A549 tumor-bearing nude mice compared with vehicle group and separately administered groups[103]. However, the still poor water solubility and the additional instability under visible light make it more difficult to translate. Moreover, we synthesized

and separated two median dianthranone compounds by further reducing the size of π-conjugated core and studied the effects of molecular skeleton structure on necrosis targeting of radioiodinated dianthrones[178]. The results demonstrated that the destruction of rigid skeleton structure dramatically reduced the necrosis targeting ability of iodine-131 labeled dianthrones and the skeleton structure of Hyp was a lead structure for further optimization of dianthrones[178], which led to the further studies of ^{131}I-HDA and ^{131}I-Shyp as described above[67,68].

Although median dianthrone compounds showed reduced necrosis targetability compared with naphthodianthrone compounds, they exhibited potential in diagnostic imaging[104–107]. A recent study demonstrated that glycosylation of sennidins had minor effect on necrosis targetability but could significantly decrease the liver uptake of tracers and improved the quality of cardiac imaging[107]. Furthermore, we found that iodine-131 labeled sennoside B and iodine-131 labeled sennidin B (Fig. 1) revealed higher necrotic-to-normal tissue ratios compared with iodine-131 labeled sennoside A and iodine-131 labeled sennidin A (Fig. 1) respectively[107], which were consistent with our previous study results[178]. On the other hand, skyrin, a dianthraquinone compound, had been designed and evaluated because it shared the same substituent groups but with severely twisted π-cores as compared with Hyp[108]. To our surprise, iodine-131 labeled skyrin (^{131}I-skyrin) (Fig. 1) exhibited comparable necrosis targeting ability with ^{131}I-Hyp (Fig. 6). Moreover, skyrin presented significantly reduced self-aggregation capacity compared with Hyp, which might explain the significantly reduced uptake of ^{131}I-skyrin in MPS[108]. In H22 tumor-bearing mice treated with CA4P, ^{131}I-skyrin showed the highest uptake in necrotic tumor with a necrotic-to-viable tumor ratio up to 11.52 ± 1.25[108], which suggested the potential for targeted radionuclide therapy of solid tumors.

In addition to our efforts, other research groups have recently identified several near-infrared fluorescent cyanines that possess necrosis avidity. The HQ5 and IRDye 800CW (Fig. 1) were demonstrated to exhibit necrosis avidity and potential for monitoring early therapeutic responses in tumors after anti-cancer

Figure 6 Representative enhanced CT and corresponding SPECT/CT images of rats with liver necrosis (large arrow) and muscle necrosis (small arrow) at 72 h after administration of 3.7 MBq of ^{131}I-skyrin or ^{131}I-Hyp. (A) Coronal images of model rats. (B) Transversal images of rat liver. (C) Transversal images of rat hind limb. Red arrows indicate the necrotic region of liver/muscle. N, necrotic area. (Reprinted with permission from Ref. 108. Copyright © 2016 American Chemical Society).

therapy[27]. The necrosis avidity mechanism of both dyes involved selective bind to cytoplasmic proteins after loss of cell membrane integrity[27]. However, the exact molecular targets need to be further elucidated. In the following study, a bimodal poly(lactic-co-glycolic acid) nanoparticle probe, encapsulating both near infrared fluorophores and perfluorocarbons, was designed to target necrotic cells by conjugation of IRDye 800CW and showed ability to specifically detect necrotic brain lesions *in vivo* by FLI and fluorine MRI[109]. Moreover, a cyanine HQ4-based multimodal imaging probe [^{111}In]DTPA-HQ4 (Fig. 1) was also developed and showed strong necrosis avidity *in vitro* and *in vivo*, which supported its potential clinical application for diagnostic purposes and monitoring efficacy of anti-cancer treatments including chemotherapy and radiotherapy[110,111]. Another near-infrared cyanine dye that shows avidity for necrotic tissues is indocyanine green (ICG) (Fig. 1). ICG was recently found to have ability to selectively bind to necrotic cells, which might be attributed to its interaction with lipoprotein and phospholipids[28]. Detection of necrotic tissues and real-time image-guided surgery were successfully achieved in different organs of different animal models by ICG FLI[28,112]. As a dye that has been approved by the U.S. Food and Drug Administration (FDA) for clinical applications, ICG potentially enable the use of optical imaging techniques for the clinical diagnosis and real-time image-guided surgical resection of necrosis-related diseases. Evans blue (EB), which has long been used as a biological dye and diagnostic agent, has also a newly discovered necrosis avid feature. Its synthetic derivative Gd-DTPA-EB (Fig. 1) had been used for *in vivo* detection of vascular endothelial injury and atherosclerotic lesions in preclinical animal models[113,114,179,180]. Although the EB is deemed to be a necrosis avid agent, the specific mechanism is still not quite clear[181].

4. Conclusion and perspectives

Over the past years, some well-defined molecular markers, but still with incompletely elucidated mechanisms, have been exploited for necrosis imaging and targeted therapy. These compounds share a common feature of necrosis avidity despite their widely diverse chemical structures and/or properties, suggesting their underlying multiple distinctive or overlapping mechanisms of action[119,120]. The clear elucidation of necrosis avid mechanisms is a prerequisite for further clinical translation and is helpful to the rational design of new and more powerful necrosis avid agents. Apart from some therapeutic strategies that have already been approved for clinical use or are currently under clinical trials, other therapeutic strategies targeting biomarkers of necrosis such as immunotherapy and extracellular histone or HMGB1-neutralizing therapy, are also being actively explored. Considering the release of multiple DAMP molecules after cell necrosis, the combined use of therapeutic agents targeting different DAMP molecules is desirable and the benefits and safety of the combination need to be further validated. Moreover, these currently identified molecules that bind to extracellular histone or HMGB1 may prove to be effective molecular scaffolds for developing imaging probes of necrosis-related diseases.

On the other hand, a number of molecular probes for imaging necrosis have been synthesized and evaluated in preclinical animal models. The potential of these probes for effective visualization of necrosis *in vivo* may benefit many areas of clinical medicine such as diagnosis of necrotic tissues and early monitoring of tumor response to treatment. Nevertheless, up to date, none of cell death imaging probes has been approved for routine clinical use. Current challenges
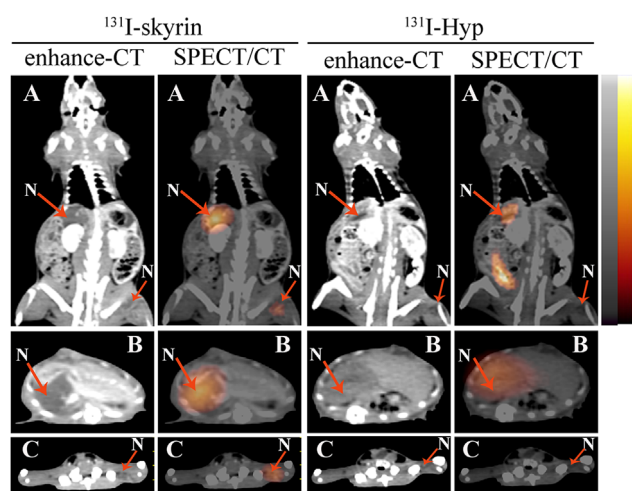
in developing necrosis imaging probes include the choice of a clinical relevant necrosis-specific biomarker, the global optimization of probe binding affinity and pharmacokinetic properties as well as the accurate detection of the temporal and spatial occurrence of necrosis. Furthermore, with the recognition that necrosis can also occur in a regulated modality[9,10,24], identifying specific biomarkers of different forms of necrosis is helpful to the development of molecular probes capable of distinguishing the specific form of necrosis. Future translational studies may primarily involve diseases where monitoring necrosis is of importance in personalized patient management, such as early evaluation of tumor responses to treatment and diagnosis of MI.

Acknowledgments

References

1. Reed GW, Rossi JE, Cannon CP. Acute myocardial infarction. *Lancet* 2017;**389**:197–210.
2. Hotchkiss RS, Tinsley KW, Karl IE. Role of apoptotic cell death in sepsis. *Scand J Infect Dis* 2003;**35**:585–92.
3. Kang R, Lotze MT, Zeh HJ, Billiar TR, Tang D. Cell death and DAMPs in acute pancreatitis. *Mol Med* 2014;**20**:466–77.
4. Mattson MP. Apoptosis in neurodegenerative disorders. *Nat Rev Mol Cell Biol* 2000;**1**:120–9.
5. Rello-Varona S, Herrero-Martin D, Lopez-Alemany R, Munoz-Pinedo C, Tirado OM. "(Not) all (dead) things share the same breath": identification of cell death mechanisms in anticancer therapy. *Cancer Res* 2015;**75**:913–7.
6. Philchenkov A. Radiation-induced cell death: signaling and pharmacological modulation. *Crit Rev Oncog* 2018;**23**:13–37.
7. Jesus Perez-Perez M, Priego E-M, Bueno O, Martins MS, Canela M-D, Liekens S. Blocking blood flow to solid tumors by destabilizing tubulin: an approach to targeting tumor growth. *J Med Chem* 2016;**59**:8685–711.
8. Galluzzi L, Vitale I, Abrams JM, Alnemri ES, Baehrecke EH, Blagosklonny MV, et al. Molecular definitions of cell death subroutines: recommendations of the Nomenclature Committee on Cell Death 2012. *Cell Death Differ* 2012;**19**:107–20.
9. Ke B, Tian M, Li J, Liu B, He G. Targeting programmed cell death using small-molecule compounds to improve potential cancer therapy. *Med Res Rev* 2016;**36**:983–1035.
10. Conrad M, Angeli JPF, Vandenabeele P, Stockwell BR. Regulated necrosis: disease relevance and therapeutic opportunities. *Nat Rev Drug Discov* 2016;**15**:348.
11. Smith BA, Smith BD. Biomarkers and molecular probes for cell death imaging and targeted therapeutics. *Bioconjugate Chem* 2012;**23**:1989–2006.
12. Neves AA, Brindle KM. Imaging cell death. *J Nucl Med* 2014;**55**:1–4.
13. Flotats A, Carrió I. Non-invasive *in vivo* imaging of myocardial apoptosis and necrosis. *Eur J Nucl Med Mol Imaging* 2003;**30**:615–30.
14. Silvestre-Roig C, de Winther MP, Weber C, Daemen MJ, Lutgens E, Soehnlein O. Atherosclerotic plaque destabilization mechanisms, models, and therapeutic strategies. *Circ Res* 2014;**114**:214–26.
15. Xia J, Yin A, Li Z, Liu X, Peng X, Xie N. Quantitative analysis of lipid-rich necrotic core in carotid atherosclerotic plaques by *in vivo* magnetic resonance imaging and clinical outcomes. *Med Sci Monit* 2017;**23**:2745–50.
16. Gonzalez L, Trigatti BL. Macrophage apoptosis and necrotic core development in atherosclerosis: a rapidly advancing field with clinical relevance to imaging and therapy. *Can J Cardiol* 2017;**33**:303–12.
17. Chen SL, Yu LK, Jiang CY, Zhao Y, Sun D, Li SY, et al. Pivotal study of iodine-131-labeled chimeric tumor necrosis treatment radioimmunotherapy in patients with advanced lung cancer. *J Clin Oncol* 2005;**23**:1538–47.
18. Croce CM, Reed JC. Finally, an apoptosis-targeting therapeutic for cancer. *Cancer Res* 2016;**76**:5914–20.
19. Hdeib A, Sloan A. Targeted radioimmunotherapy: the role of ^{131}I-chTNT-1/B mAb (Cotara®) for treatment of high-grade gliomas. *Future Oncol* 2012;**8**:659–69.
20. Wang K, Na MH, Hoffman AS, Shim G, Han SE, Oh YK, Kwon IC, et al. *In situ* dose amplification by apoptosis-targeted drug delivery. *J Control Release* 2011;**154**:214–7.
21. He X, Bonaparte N, Kim S, Acharya B, Lee JY, Chi L, et al. Enhanced delivery of T cells to tumor after chemotherapy using membrane-anchored, apoptosis-targeted peptide. *J Control Release* 2012;**162**:521–8.
22. Zeng W, Wang X, Xu P, Liu G, Eden HS, Chen X. Molecular imaging of apoptosis: from micro to macro. *Theranostics* 2015;**5**:559–82.
23. Savla R, Minko T. Nanoparticle design considerations for molecular imaging of apoptosis: diagnostic, prognostic, and therapeutic value. *Adv Drug Deliv Rev* 2017;**113**:122–40.
24. Moreno-Gonzalez G, Vandenabeele P, Krysko DV. Necroptosis: a novel cell death modality and its potential relevance for critical care medicine. *Am J Resp Crit Care* 2016;**194**:415–28.
25. Parseghian MH, Mechetner E, Osidak MS, Domogatskii SP. Application of monoclonal antibodies for the diagnostic and therapeutic targeting of human tumors with a necrotic component. *Russ J Gen Chem* 2014;**84**:345–56.
26. Cona MM, Oyen R, Ni Y. Necrosis avidity of organic compounds: a natural phenomenon with exploitable theragnostic potentials. *Curr Med Chem* 2015;**22**:1829–49.
27. Xie B, Stammes MA, van Driel PBAA, Cruz LJ, Knol-Blankevoort VT, Lowik MAM, et al. Necrosis avid near infrared fluorescent cyanines for imaging cell death and their use to monitor therapeutic efficacy in mouse tumor models. *Oncotarget* 2015;**6**:39036–49.
28. Fang C, Wang K, Zeng C, Chi C, Shang W, Ye J, et al. Illuminating necrosis: from mechanistic exploration to preclinical application using fluorescence molecular imaging with indocyanine green. *Sci Rep* 2016;**6**:21013.
29. Patel SJ, Shapiro WR, Laske DW, Jensen RL, Asher AL, Wessels BW, et al. Safety and feasibility of convection-enhanced delivery of cotara for the treatment of malignant glioma: initial experience in 51 patients. *Neurosurgery* 2005;**56**:1243–52.
30. Shapiro WR, Carpenter SP, Roberts K, Shan JS. ^{131}I-chTNT-1/B mAb: tumour necrosis therapy for malignant astrocytic glioma. *Exp Opin Biol Ther* 2006;**6**:539–45.
31. Hdeib A, Sloan AE. Convection-enhanced delivery of ^{131}I-chTNT-1/B mAB for treatment of high-grade adult gliomas. *Exp Opin Biol Ther* 2011;**11**:799–806.
32. Ye L, Fan J, Shi X, Tao Q, Ye D, Xian Z, et al. Tumor necrosis therapy antibody interleukin-2 fusion protein elicits prolonged and targeted antitumor effects *in vivo*. *Appl Microbiol Biot* 2014;**98**:4053–61.
33. Fallon J, Tighe R, Kradjian G, Guzman W, Bernhardt A, Neuteboom B, et al. The immunocytokine NHS-IL12 as a potential cancer therapeutic. *Oncotarget* 2014;**5**:1869–84.
34. Schilbach K, Alkhaled M, Welker C, Eckert F, Blank G, Ziegler H, et al. Cancer-targeted IL-12 controls human rhabdomyosarcoma by senescence induction and myogenic differentiation. *Oncoimmunology* 2015;**4**:e1014760.
35. Eckert F, Schmitt J, Zips D, Krueger MA, Pichler BJ, Gillies SD, et al. Enhanced binding of necrosis-targeting immunocytokine NHS-IL12 after local tumour irradiation in murine xenograft models. *Cancer Immunol Immun* 2016;**65**:1003–13.
36. Eckert F, Jelas I, Oehme M, Huber SM, Sonntag K, Welker C, et al. Tumor-targeted IL-12 combined with local irradiation leads to systemic tumor control *via* abscopal effects *in vivo*. *Oncoimmunology* 2017;**6**:e1323161.
37. Fallon JK, Vandeveer AJ, Schlom J, Greiner JW. Enhanced antitumor effects by combining an IL-12/anti-DNA fusion protein with avelumab, an anti-PD-L1 antibody. *Oncotarget* 2017;**8**:20558–71.

38. Xu C, Zhang Y, Rolfe PA, Hernandez VM, Guzman W, Kradjian G, et al. Combination therapy with NHS-muIL12 and avelumab (anti-PD-L1) enhances antitumor efficacy in preclinical cancer models. *Clin Cancer Res* 2017;**23**:5869–80.

39. Hornick JL, Sharifi J, Khawli LA, Hu PS, Bai WG, Alauddin MM, et al. Single amino acid substitution in the Fc region of chimeric TNT-3 antibody accelerates clearance and improves immunoscintigraphy of solid tumors. *J Nucl Med* 2000;**41**:355–62.

40. Khawli LA, Alauddin MM, Hu PS, Epstein AL. Tumor targeting properties of indium-111 labeled genetically engineered Fab′ and F(ab′)₂ constructs of chimeric tumor necrosis treatment (chTNT)-3 antibody. *Cancer Biother Radiopharm* 2003;**18**:931–40.

41. Khawli LA, Biela B, Hu PS, Epstein AL. Comparison of recombinant derivatives of chimeric TNT-3 antibody for the radioimaging of solid tumors. *Hybrid Hybridom* 2003;**22**:1–9.

42. Jang JK, Khawli LA, Park R, Wu BW, Li Z, Canter D, et al. Cytoreductive chemotherapy improves the biodistribution of antibodies directed against tumor necrosis in murine solid tumor models. *Mol Cancer Ther* 2013;**12**:2827–36.

43. Tu J, Ji J, Wu F, Wang Y, Zhang D, Zhao Z, et al. Effectiveness of combined ^{131}I-chTNT and radiofrequency ablation therapy in treating advanced hepatocellular carcinoma. *Cell Biochem Biophys* 2015;**71**:777–84.

44. Bryan RA, Jiang Z, Jandl T, Strauss J, Koba W, Onyedika C, et al. Treatment of experimental pancreatic cancer with 213-Bismuth-labeled chimeric antibody to single-strand DNA. *Exp Rev Anticancer Ther* 2014;**14**:1243–9.

45. Jang JK, Chretin J, Bruyette D, Hu P, Epstein AL. Phase 1 dose-escalation study with LEC/chTNT-3 and toceranib phosphate (Palladia®) in dogs with spontaneous malignancies. *J Cancer Sci Ther* 2015;**7**:167–74.

46. Jang JK, Khawli LA, Canter DC, Hu P, Zhu TH, Wu BW, et al. Systemic delivery of chTNT-3/CpG immunoconjugates for immunotherapy in murine solid tumor models. *Cancer Immunol Immun* 2016;**65**:511–23.

47. Garanger E, Hilderbrand SA, Blois JT, Sosnovik DE, Weissleder R, Josephson L. A DNA-binding Gd chelate for the detection of cell death by MRI. *Chem Commun* 2009:4444–6.

48. Huang S, Chen HH, Yuan H, Dai G, Schuhle DT, Mekkaoui C, et al. Molecular MRI of acute necrosis with a novel DNA-binding gadolinium chelate: kinetics of cell death and clearance in infarcted myocardium. *Circ Cardiovasc Imag* 2011;**4**:729–37.

49. Dasari M, Lee S, Sy J, Kim D, Lee S, Brown M, et al. Hoechst-IR: an imaging agent that detects necrotic tissue *in vivo* by binding extracellular DNA. *Org Lett* 2010;**12**:3300–3.

50. Dasari M, Acharya AP, Kim D, Lee S, Lee S, Rhea J, et al. H-Gemcitabine: a new gemcitabine prodrug for treating cancer. *Bioconjugate Chem* 2013;**24**:4–8.

51. Khan RS, Martinez MD, Sy JC, Pendergrass KD, Che P-l, Brown ME, et al. Targeting extracellular DNA to deliver IGF-1 to the injured heart. *Sci Rep* 2014;**4**:4257.

52. Kim S, Park J, Youn YS, Oh KT, Bae JH, Lee ES. Hoechst 33258-conjugated hyaluronated fullerene for efficient photodynamic tumor therapy and necrotic tumor targeting. *J Bioact Compat Pol* 2015;**30**:275–88.

53. Zhang D, Gao M, Yao N, Jiang C, Liu W, Li T, et al. Preclinical evaluation of radioiodinated Hoechst 33258 for early prediction of tumor response to treatment of vascular-disrupting agents. *Contrast Media Mol Imaging* 2018;**2018**: Article ID 5237950.

54. Fonge H, Vunckx K, Wang H, Feng Y, Mortelmans L, Nuyts J, et al. Non-invasive detection and quantification of acute myocardial infarction in rabbits using mono-[^{123}I]iodohypericin µSPECT. *Eur Heart J* 2008;**29**:260–9.

55. Feng Y, Cona MM, Vunckx K, Li Y, Chen F, Nuyts J, et al. Detection and quantification of acute reperfused myocardial infarction in rabbits using DISA-SPECT/CT and 3.0 T cardiac MRI. *Int J Cardiol* 2013;**168**:4191–8.

56. Cona MM, Feng Y, Li Y, Chen F, Vunckx K, Zhou L, et al. Comparative study of iodine-123-labeled hypericin and Tc-99m-labeled hexakis 2-methoxy isobutyl isonitrile in a rabbit model of myocardial infarction. *J Cardiovasc Pharm* 2013;**62**:304–11.

57. Li J, Sun Z, Zhang J, Shao H, Cona MM, Wang H, et al. A dual-targeting anticancer approach: soil and seed principle. *Radiology* 2011;**260**:799–807.

58. Song S, Xiong C, Zhou M, Lu W, Huang Q, Ku G, et al. Small-animal PET of tumor damage induced by photothermal ablation with ^{64}Cu-Bis-DOTA-hypericin. *J Nucl Med* 2011;**52**:792–9.

59. Van de Putte M, Marysael T, Fonge H, Roskams T, Cona MM, Li J, et al. Radiolabeled iodohypericin as tumor necrosis avid tracer: diagnostic and therapeutic potential. *Int J Cancer* 2012;**131**:E129–37.

60. Li J, Cona MM, Chen F, Feng Y, Zhou L, Yu J, et al. Exploring theranostic potentials of radioiodinated hypericin in rodent necrosis models. *Theranostics* 2012;**2**:1010–9.

61. Li J, Cona MM, Chen F, Feng Y, Zhou L, Zhang G, et al. Sequential systemic administrations of combretastatin A4 phosphate and radioiodinated hypericin exert synergistic targeted theranostic effects with prolonged survival on SCID mice carrying bifocal tumor xenografts. *Theranostics* 2013;**3**:127–37.

62. Liu W, Zhang D, Feng Y, Li Y, Huang D, Jiang C, et al. Biodistribution and anti-tumor efficacy of intratumorally injected necrosis-avid theranostic agent radioiodinated hypericin in rodent tumor models. *J Drug Target* 2015;**23**:371–9.

63. Zhu M, Lin X-A, Zha X-M, Zhou W-B, Xia T-S, Wang S. Evaluation of the therapeutic efficacy of sequential therapy involving percutaneous microwave ablation in combination with ^{131}I-hypericin using the VX2 rabbit breast solid tumor model. *PLoS One* 2015;**10**: e0120303.

64. Shao H, Zhang J, Sun Z, Chen F, Dai X, Li Y, et al. Necrosis targeted radiotherapy with iodine-131-labeled hypericin to improve anticancer efficacy of vascular disrupting treatment in rabbit VX2 tumor models. *Oncotarget* 2015;**6**:14247–59.

65. Gao L, Zhang J, Ma T, Yao N, Gao M, Shan X, et al. Improved therapeutic outcomes of thermal ablation on rat orthotopic liver allograft sarcoma models by radioiodinated hypericin induced necrosis targeted radiotherapy. *Oncotarget* 2016;**7**:51450–61.

66. Cona MM, de Witte P, Verbruggen A, Ni Y. An overview of translational (radio)pharmaceutical research related to certain onco-logical and non-oncological applications. *World J Methodol* 2013;**3**:45–64.

67. Li J, Zhang J, Yang S, Jiang C, Zhang D, Jin Q, et al. Synthesis and preclinical evaluation of radioiodinated hypericin dicarboxylic acid as a necrosis avid agent in rat models of induced hepatic, muscular, and myocardial necroses. *Mol Pharm* 2016;**13**:232–40.

68. Duan X, Yin Z, Jiang C, Jin Q, Zhang D, Sun Z, et al. Radio-iodinated hypericin disulfonic acid sodium salts as a DNA-binding probe for early imaging of necrotic myocardium. *Eur J Pharm Biopharm* 2017;**117**:151–9.

69. Jin Q, Zhao J, Gao M, Feng Y, Liu W, Yin Z, et al. Evaluation of necrosis avidity and potential for rapid imaging of necrotic myocardium of radioiodinated hypocrellins. *Mol Imaging Biol* 2018;**20**:551–61.

70. Wang Q, Yang S, Jiang C, Li J, Wang C, Chen L, et al. Discovery of radioiodinated monomeric anthraquinones as a novel class of necrosis avid agents for early imaging of necrotic myocardium. *Sci Rep* 2016;**6**:21341.

71. Luo Q, Jin Q, Su C, Zhang D, Jiang C, Fish AF, et al. Radiolabeled rhein as small-molecule necrosis avid agents for imaging of necrotic myocardium. *Anal Chem* 2017;**89**:1260–6.

72. Ji A-Y, Jin Q-M, Zhang D-J, Zhu H, Su C, Duan X-H, et al. Novel ^{18}F-labeled 1-hydroxyanthraquinone derivatives for necrotic myocardium imaging. *ACS Med Chem Lett* 2017;**8**:191–5.

73. Su C, Zhang D, Bao N, Ji A, Feng Y, Chen L, et al. Evaluation of radioiodinated 1,4-naphthoquinones as necrosis avid agents for rapid myocardium necrosis imaging. *Mol Imaging Biol* 2018;**20**:74–84.

74. Liang J, Sun Z, Zhang D, Jin Q, Cai L, Ma L, et al. First evaluation of radioiodinated flavonoids as necrosis-avid agents and application in early assessment of tumor necrosis. *Mol Pharm* 2018;**15**:207–15.

75. Xie BW, Park D, Van Beek ER, Blankevoort V, Orabi Y, Que I, et al. Optical imaging of cell death in traumatic brain injury using a heat shock protein-90 alkylator. *Cell Death Dis* 2013;**4**:e473.

76. Park D, Xie B-W, Van Beek ER, Blankevoort V, Que I, Lowik CWGM, et al. Optical imaging of treatment-related tumor cell death using a heat shock protein-90 alkylator. *Mol Pharm* 2013;**10**:3882–91.

77. Tahara N, Zandbergen HR, de Haas HJ, Petrov A, Pandurangi R, Yamaki T, et al. Noninvasive molecular imaging of cell death in myocardial infarction using ^{111}In-GSAO. *Sci Rep* 2014;**4**:6826.

78. Yamaki T, de Haas HJ, Tahara N, Petrov A, Mohar D, Haider N, et al. Cardioprotection by minocycline in a rabbit model of ischemia/reperfusion injury: detection of cell death by *in vivo* ^{111}In-GSAO SPECT. *J Nucl Cardiol* 2018;**25**:94–100.

79. Park D, Don AS, Massamiri T, Karwa A, Warner B, MacDonald J, et al. Noninvasive imaging of cell death using an Hsp90 ligand. *J Am Chem Soc* 2011;**133**:2832–5.

80. Staudacher AH, Al-Ejeh F, Fraser CK, Darby JM, Roder DM, Ruszkiewicz A, et al. The La antigen is over-expressed in lung cancer and is a selective dead cancer cell target for radioimmunotherapy using the La-specific antibody APOMAB[®]. *EJNMMI Res* 2014;**4**:2.

81. Al-Ejeh F, Darby JM, Brown MP. Chemotherapy synergizes with radioimmunotherapy targeting La autoantigen in tumors. *PLoS One* 2009;**4**:e4630.

82. Al-Ejeh F, Darby JM, Tsopelas C, Smyth D, Manavis J, Brown MP. APOMAB[®], a La-specific monoclonal antibody, detects the apoptotic tumor response to life-prolonging and DNA-damaging chemotherapy. *PLoS One* 2009;**4**:e4558.

83. Staudacher AH, Bezak E, Borysenko A, Brown MP. Targeted alpha-therapy using [227]Th-APOMAB and cross-fire antitumour effects: preliminary *in-vivo* evaluation. *Nucl Med Commun* 2014;**35**:1284–90.

84. Sadeghi H, Rahmanian N, Amiri FT, Amirfakhrian H, Abedi SM, Hosseinimehr SJ. ^{99m}Tc-Glucarate for assessment of paclitaxel therapy in human ovarian cancer in mice. *Iran J Basic Med Sci* 2018;**21**:77–82.

85. Wildhagen KCAA, Garcia de Frutos P, Reutelingsperger CP, Schrijver R, Areste C, Ortega-Gomez A, et al. Nonanticoagulant heparin prevents histone-mediated cytotoxicity *in vitro* and improves survival in sepsis. *Blood* 2014;**123**:1098–101.

86. Wang F, Zhang N, Li B, Liu L, Ding L, Wang Y, et al. Heparin defends against the toxicity of circulating histones in sepsis. *Front Biosci* 2015;**20**:1259–70.

87. Nagano F, Mizuno T, Mizumoto S, Yoshioka K, Takahashi K, Tsuboi N, et al. Chondroitin sulfate protects vascular endothelial cells from toxicities of extracellular histones. *Eur J Pharm* 2018;**826**:48–55.

88. Xu J, Zhang X, Pelayo R, Monestier M, Ammollo CT, Semeraro F, et al. Extracellular histones are major mediators of death in sepsis. *Nat Med* 2009;**15**:1318–21.

89. Xu J, Zhang X, Monestier M, Esmon NL, Esmon CT. Extracellular histones are mediators of death through TLR2 and TLR4 in mouse fatal liver injury. *J Immunol* 2011;**187**:2626–31.

90. Allam R, Scherbaum CR, Darisipudi MN, Mulay SR, Haegele H, Lichtnekert J, et al. Histones from dying renal cells aggravate kidney injury *via* TLR2 and TLR4. *J Am Soc Nephrol* 2012;**23**:1375–88.

91. Venereau E, De Leo F, Mezzapelle R, Careccia G, Musco G, Bianchi ME. HMGB1 as biomarker and drug target. *Pharm Res* 2016;**111**:534–44.

92. Ugrinova I, Pasheva E. HMGB1 protein: a therapeutic target inside and outside the cell. *Adv Protein Chem Struct Biol* 2017;**107**:37–76.

93. Andersson U, Yang H, Harris H. Extracellular HMGB1 as a therapeutic target in inflammatory diseases. *Exp Opin Ther Targets* 2018;**22**:263–77.

94. Lundback P, Lea JD, Sowinska A, Ottosson L, Furst CM, Steen J, et al. A novel high mobility group box 1 neutralizing chimeric antibody attenuates drug-induced liver injury and postinjury inflammation in mice. *Hepatology* 2016;**64**:1699–710.

95. Musumeci D, Roviello GN, Montesarchio D. An overview on HMGB1 inhibitors as potential therapeutic agents in HMGB1-related pathologies. *Pharmacol Ther* 2014;**141**:347–57.

96. Horiuchi T, Sakata N, Narumi Y, Kimura T, Hayashi T, Nagano K, et al. Metformin directly binds the alarmin HMGB1 and inhibits its proinflammatory activity. *J Biol Chem* 2017;**292**:8436–46.

97. Gallagher FA, Kettunen MI, Hu D-E, Jensen PR, in't Zandt R, Karlsson M, et al. Production of hyperpolarized $[1,4-^{13}C_2]$malate from $[1,4-^{13}C_2]$fumarate is a marker of cell necrosis and treatment response in tumors. *Proc Natl Acad Sci U S A* 2009;**106**:19801–6.

98. Witney TH, Kettunen MI, Hu De, Gallagher FA, Bohndiek SE, Napolitano R, et al. Detecting treatment response in a model of human breast adenocarcinoma using hyperpolarised $[1-^{13}C]$pyruvate and $[1,4-^{13}C_2]$fumarate. *Br J Cancer* 2010;**103**:1400–6.

99. Clatworthy MR, Kettunen MI, Hu D-E, Mathews RJ, Witney TH, Kennedy BWC, et al. Magnetic resonance imaging with hyperpolarized $[1,4-^{13}C_2]$fumarate allows detection of early renal acute tubular necrosis. *Proc Natl Acad Sci U S A* 2012;**109**:13374–9.

100. Miller JJ, Lau AZ, Nielsen PM, McMullen-Klein G, Lewis AJ, Jespersen NR, et al. Hyperpolarized $[1,4-^{13}C_2]$fumarate enables magnetic resonance-based imaging of myocardial necrosis. *JACC-Cardiovasc Imag* 2018;**11**:1594–606.

101. Feuerecker B, Durst M, Michalik M, Schneider G, Saur D, Menzel M, et al. Hyperpolarized ^{13}C diffusion MRS of co-polarized pyruvate and fumarate to measure lactate export and necrosis. *J Cancer* 2017;**8**:3078–85.

102. Liu X, Feng Y, Jiang C, Lou B, Li Y, Liu W, et al. Radiopharmaceutical evaluation of ^{131}I-protohypericin as a necrosis avid compound. *J Drug Target* 2015;**23**:417–26.

103. Liu X, Jiang C, Zhang D, Gao M, Peng F, Huang D, et al. Tumor necrosis targeted radiotherapy of non-small cell lung cancer using radioiodinated protohypericin in a mouse model. *Oncotarget* 2015;**6**:26400–10.

104. Ji Y, Jiang C, Zhang X, Liu W, Gao M, Li Y, et al. Necrosis-targeted combinational theragnostic approach to treat cancer. *Oncotarget* 2014;**5**:2934–46.

105. Jiang C, Gao M, Li Y, Huang D, Yao N, Ji Y, et al. Exploring diagnostic potentials of radioiodinated sennidin A in rat model of reperfused myocardial infarction. *Int J Pharm* 2015;**495**:31–40.

106. Zhang D, Huang D, Ji Y, Jiang C, Li Y, Gao M, et al. Experimental evaluation of radioiodinated sennoside B as a necrosis-avid tracer agent. *J Drug Target* 2015;**23**:180–90.

107. Li L, Zhang D, Yang S, Song S, Li J, Wang Q, et al. Effects of glycosylation on biodistribution and imaging quality of necrotic myocardium of iodine-131-labeled sennidins. *Mol Imaging Biol* 2016;**18**:877–86.

108. Wang C, Jin Q, Yang S, Zhang D, Wang Q, Li J, et al. Synthesis and evaluation of ^{131}I-skyrin as a necrosis avid agent for potential targeted radionuclide therapy of solid tumors. *Mol Pharm* 2016;**13**:180–9.

109. Cruz LJ, Que I, Aswendt M, Chan A, Hoehn M, Lowik C. Targeted nanoparticles for the non-invasive detection of traumatic brain injury by optical imaging and fluorine magnetic resonance imaging. *Nano Res* 2016;**9**:1276–89.

110. Stammes MA, Knol-Blankevoort VT, Cruz LJ, Feitsma HRIJ, Mezzanotte L, Cordfunke RA, et al. Pre-clinical evaluation of a cyanine-based SPECT probe for multimodal tumor necrosis imaging. *Mol Imaging Biol* 2016;**18**:905–15.

111. Stammes MA, Maeda A, Bu J, Scollard DA, Kulbatski I, Medeiros PJ, et al. The necrosis-avid small molecule HQ4-DTPA as a multi-modal imaging agent for monitoring radiation therapy-induced tumor cell death. *Front Oncol* 2016;**6**:221.

112. Sonin D, Papayan G, Pochkaeva E, Chefu S, Minasian S, Kurapeev D, et al. *In vivo* visualization and *ex vivo* quantification of experimental myocardial infarction by indocyanine green fluorescence imaging. *Biomed Opt Express* 2017;**8**:151–61.

113. Yamamoto T, Ikuta K, Oi K, Abe K, Uwatoku T, Hyodo F, et al. *In vivo* MR detection of vascular endothelial injury using a new class of MRI contrast agent. *Bioorg Med Chem Lett* 2004;**14**:2787–90.

114. Yasuda S, Ikuta K, Uwatoku T, Oi K, Abe K, Hyodo F, et al. *In vivo* magnetic resonance imaging of atherosclerotic lesions with a newly developed evans blue-DTPA-Gadolinium contrast medium in apolipoprotein-E-deficient mice. *J Vasc Res* 2008;**45**:123–8.

115. Al-Ejeh F, Staudacher AH, Smyth DR, Darby JM, Denoyer D, Tsopelas C, et al. Postchemotherapy and tumor-selective targeting with the La-specific DAB4 monoclonal antibody relates to apoptotic cell clearance. *J Nucl Med* 2014;**55**:772–9.

116. Wu DC, Ingram A, Lahti JH, Mazza B, Grenet J, Kapoor A, et al. Apoptotic release of histones from nucleosomes. *J Biol Chem* 2002;**277**:12001–8.

117. Kang R, Chen R, Zhang Q, Hou W, Wu S, Cao L, et al. HMGB1 in health and disease. *Mol Asp Med* 2014;**40**:1–116.

118. Khawli LA, Hu P, Epstein AL. Multiple uses of tumor necrosis therapy (TNT) for the treatment and imaging of solid tumors: preclinical considerations and progress. *Update Cancer Ther* 2006;**1**:33–47.

119. Ni Y, Bormans G, Chen F, Verbruggen A, Marchal G. Necrosis avid contrast agents: functional similarity *versus* structural diversity. *Invest Radiol* 2005;**40**:526–35.

120. Ni Y. Metalloporphyrins and functional analogues as MRI contrast agents. *Curr Med Imaging Rev* 2008;**4**:96–112.

121. Epstein AL, Chen FM, Taylor CR. A novel method for the detection of necrotic lesions in human cancers. *Cancer Res* 1988;**48**:5842–8.

122. Miller GK, Naeve GS, Gaffar SA, Epstein AL. Immunologic and biochemical analysis of TNT-1 and TNT-2 monoclonal antibody binding to histones. *Hybridoma* 1993;**12**:689–98.

123. Anderson PM, Wiseman GA, Lewis BD, Charboneau JW, Dunn WL, Carpenter SP, et al. A phase I safety and imaging study using radiofrequency ablation (RFA) followed by ^{131}I-chTNT-1/B radio-immunotherapy adjuvant treatment of hepatic metastases. *Cancer Ther* 2003;**1**:297–306.

124. Khawli LA, Mizokami MM, Sharifi J, Hu PS, Epstein AL. Pharmacokinetic characteristics and biodistribution of radioiodinated chimeric TNT-1,-2, and-3, monoclonal antibodies after chemical modification with biotin. *Cancer Biother Radio* 2002;**17**:359–70.

125. Sharifi J, Khawli LA, Hu P, King S, Epstein AL. Characterization of a phage display-derived human monoclonal antibody (NHS76) counterpart to chimeric TNT-1 directed against necrotic regions of solid tumors. *Hybrid Hybridom* 2001;**20**:305–12.

126. Hornick JL, Sharifi J, Khawli LA, Hu PS, Biela BH, Mizokami MM, et al. A new chemically modified chimeric TNT-3 monoclonal antibody directed against DNA for the radioimmunotherapy of solid tumors. *Cancer Biother Radio* 1998;**13**:255–68.

127. Zheng S, Xu H, Lu M, Yue D, Xie X, Liu G. Radiofrequency ablation before intratumoral injection of ^{131}I-chTNT improves the tumor-to-normal tissue ratio in solid VX2 tumor. *Cancer Biother Radiopharm* 2013;**28**:725–30.

128. Jendzelovska Z, Jendzelovsky R, Kucharova B, Fedorocko P. Hypericin in the light and in the dark: two sides of the same coin. *Front Plant Sci* 2016;**7**:560.

129. Liu X, Jiang C, Li Y, Liu W, Yao N, Gao M, et al. Evaluation of hypericin: effect of aggregation on targeting biodistribution. *J Pharm Sci* 2015;**104**:215–22.

130. Chen Z, Lohr A, Saha-Moeller CR, Wuerthner F. Self-assembled pi-stacks of functional dyes in solution: structural and thermodynamic features. *Chem Soc Rev* 2009;**38**:564–84.

131. Chen Z, Fimmel B, Wuerthner F. Solvent and substituent effects on aggregation constants of perylene bisimide π-stacks—a linear free energy relationship analysis. *Org Biomol Chem* 2012;**10**:5845–55.

132. Yang Y, Ji S, Liu S. Impact of multiple negative charges on blood clearance and biodistribution characteristics of ^{99m}Tc-labeled dimeric cyclic RGD peptides. *Bioconjugate Chem* 2014;**25**:1720–9.

133. Haskali MB, Denoyer D, Noonan W, Culinane C, Rangger C, Pouliot N, et al. Sulfonation of tyrosine as a method to improve biodistribution of peptide-based radiotracers: novel ^{18}F-labeled cyclic RGD analogues. *Mol Pharm* 2017;**14**:1169–80.

134. Chen Z, Baumeister U, Tschierske C, Wuerthner F. Effect of core twisting on self-assembly and optical properties of perylene bisimide dyes in solution and columnar liquid crystalline phases. *Chem Eur J* 2007;**13**:450–65.

135. Priebe W, Fokt I, Przewloka T, Chaires JB, Portugal J, Trent JO. Exploiting anthracycline scaffold for designing DNA-targeting agents. *Method Enzymol* 2001;**340**:529–55.

136. Strekowski L, Wilson B. Noncovalent interactions with DNA: an overview. *Mutat Res-Fund Mol* 2007;**623**:3–13.

137. Sun Y, Bi S, Song D, Qiao C, Mu D, Zhang H. Study on the interaction mechanism between DNA and the main active components in *Scutellaria baicalensis* Georgi. *Sens Actuat B Chem* 2008;**129**:799–810.

138. Hahn J-S. The Hsp90 chaperone machinery: from structure to drug development. *BMB Rep* 2009;**42**:623–30.

139. Goetz MP, Toft DO, Ames MM, Erlichman C. The Hsp90 chaperone complex as a novel target for cancer therapy. *Ann Oncol* 2003;**14**:1169–76.

140. Dilda PJ, Hogg PJ. Arsenical-based cancer drugs. *Cancer Treat Rev* 2007;**33**:542–64.

141. Intine RV, Tenenbaum SA, Sakulich AL, Keene JD, Maraia RJ. Differential phosphorylation and subcellular localization of and La RNPs associated with precursor tRNAs and translation-related mRNAs. *Mol Cell* 2003;**12**:1301–7.

142. Al-Ejeh F, Darby JM, Brown MP. The La autoantigen is a malignancy-associated cell death target that is induced by DNA-damaging drugs. *Clin Cancer Res* 2007;**13**:5509S–18S.

143. Al-Ejeh F, Darby JM, Pensa K, Diener KR, Hayball JD, Brown MP. *In vivo* targeting of dead tumor cells in a murine tumor model using a monoclonal antibody specific for the La autoantigen. *Clin Cancer Res* 2007;**13**:5519S–27S.

144. Al Darwish R, Staudacher AH, Bezak E, Brown MP. Autoradio-graphy imaging in targeted α therapy with timepix detector. *Comput Math Method Med* 2015;**2015**:Article ID 612580.

145. Penfold SN, Brown MP, Staudacher AH, Bezak E. Monte Carlo simulations of dose distributions with necrotic tumor targeted radio-immunotherapy. *Appl Radiat Isot* 2014;**90**:40–5.

146. Allam R, Kumar SVR, Darisipudi MN, Anders H-J. Extracellular histones in tissue injury and inflammation. *J Mol Med* 2014;**92**:465–72.

147. Chen R, Kang R, Fan XG, Tang D. Release and activity of histone in diseases. *Cell Death Dis* 2014;**5**:e1370.

148. Silk E, Zhao H, Weng H, Ma D. The role of extracellular histone in organ injury. *Cell Death Dis* 2017;**8**:e2812.

149. Kawai C, Kotani H, Miyao M, Ishida T, Jemail L, Abiru H, et al. Circulating extracellular histones are clinically relevant mediators of multiple organ injury. *Am J Pathol* 2016;**186**:829–43.

150. Lv X, Wen T, Song J, Xie D, Wu L, Jiang X, et al. Extracellular histones are clinically relevant mediators in the pathogenesis of acute respiratory distress syndrome. *Resp Res* 2017;**18**:165.

151. Yang R, Zou X, Tenhunen J, Tonnessen TI. HMGB1 and extra-cellular histones significantly contribute to systemic inflammation and multiple organ failure in acute liver failure. *Mediat Inflamm* 2017;**2017**:Article ID 5928078.

152. Khaw BA, Nakazawa A, Odonnell SM, Pak KY, Narula J. Avidity of technetium 99m glucarate for the necrotic myocardium: *in vivo* and *in vitro* assessment. *J Nucl Cardiol* 1997;**4**:283–90.

153. Yaoita H, Uehara T, Brownell AL, Rabito CA, Ahmad M, Khaw BA, et al. Localization of technetium-99m-glucarate in zones of acute cerebral injury. *J Nucl Med* 1991;**32**:272–8.

154. Perek N, Sabido O, Le Jeune N, Prevot N, Vergnon J-M, Clotagatide A, et al. Could ^{99m}Tc-glucarate be used to evaluate tumour necrosis?. *Eur J Nucl Med Mol Imaging* 2008;**35**:1290–8.

155. Choudhury PS, Savio E, Solanki KK, Alonso O, Gupta A, Gambini JP, et al. [99m]Tc Glucarate as a potential radiopharmaceutical agent for

assessment of tumor viability: from bench to the bed side. *World J Nucl Med* 2012;**11**:47–56.

156. Huang H, Chen H-W, Evankovich J, Yan W, Rosborough BR, Nace GW, et al. Histones activate the NLRP3 inflammasome in kupffer cells during sterile inflammatory liver injury. *J Immunol* 2013;**191**:2665–79.

157. Abrams ST, Zhang N, Manson J, Liu T, Dart C, Baluwa F, et al. Circulating histones are mediators of trauma-associated lung injury. *Am J Resp Crit Care* 2013;**187**:160–9.

158. Bosmann M, Grailer JJ, Ruemmler R, Russkamp NF, Zetoune FS, Sarma JV, et al. Extracellular histones are essential effectors of C5aR- and C5L2-mediated tissue damage and inflammation in acute lung injury. *FASEB J* 2013;**27**:5010–21.

159. Raucci A, Palumbo R, Bianchi ME. HMGB1: a signal of necrosis. *Autoimmunity* 2007;**40**:285–9.

160. Gauley J, Pisetsky DS. The translocation of HMGB1 during cell activation and cell death. *Autoimmunity* 2009;**42**:299–301.

161. Zitvogel L, Kepp O, Kroemer G. Decoding cell death dignals in inflammation and immunity. *Cell* 2010;**140**:798–804.

162. Chen Q, Guan X, Zuo X, Wang J, Yin W. The role of high mobility group box 1 (HMGB1) in the pathogenesis of kidney diseases. *Acta Pharm Sin B* 2016;**6**:183–8.

163. Wang Y, Zhong J, Zhang X, Liu Z, Yang Y, Gong Q, et al. The role of HMGB1 in the pathogenesis of type 2 diabetes. *J Diabetes Res* 2016;**2016**:Article ID 2543268.

164. Angelopoulou E, Piperi C, Adamopoulos C, Papavassiliou AG. Pivotal role of high-mobility group box 1 (HMGB1) signaling pathways in glioma development and progression. *J Mol Med* 2016;**94**:867–74.

165. Wu H, Chen Z, Xie J, Kang L-N, Wang L, Xu B. High mobility group box-1: a missing link between diabetes and its complications. *Mediat Inflamm* 2016;**2016**:Article ID 3896147.

166. Wan W, Cao L, Khanabdali R, Kalionis B, Tai X, Xia S. The emerging role of HMGB1 in neuropathic pain: a potential therapeutic target for neuroinflammation. *J Immunol Res* 2016;**2016**:Article ID 6430423.

167. Ding J, Cui X, Liu Q. Emerging role of HMGB1 in lung diseases: friend or foe. *J Cell Mol Med* 2017;**21**:1046–57.

168. Austin Huy N, Detty SQ, Agrawal DK. Clinical implications of high-mobility group box-1 (HMGB1) and the receptor for advanced glycation end-products (RAGE) in cutaneous malignancy: a systematic review. *Anticancer Res* 2017;**37**:1–7.

169. Yamamoto T, Tajima Y. HMGB1 is a promising therapeutic target for acute liver failure. *Exp Rev Gastroenterol Hepatol* 2017;**11**:673–82.

170. Tian X, Liu C, Shu Z, Chen G. Review: therapeutic targeting of HMGB1 in stroke. *Curr Drug Deliv* 2017;**14**:785–90.

171. Nelson SJ, Kurhanewicz J, Vigneron DB, Larson PEZ, Harzstark AL, Ferrone M, et al. Metabolic imaging of patients with prostate cancer using hyperpolarized [1-^{13}C]pyruvate. *Sci Transl Med* 2013;**5**:198ra108.

172. Cunningham CH, Lau JYC, Chen AP, Geraghty BJ, Perks WJ, Roifman I, et al. Hyperpolarized ^{13}C metabolic MRI of the human heart initial experience. *Circ Res* 2016;**119**:1177–82.

173. Ji Y, Zhan Y, Jiang C, Jiang X, Gao M, Liu W, et al. Improvement of solubility and targetability of radioiodinated hypericin by using sodium cholate based solvent in rat models of necrosis. *J Drug Target* 2014;**22**:304–12.

174. Cona MM, Feng Y, Zhang J, Li Y, Verbruggen A, Oyen R, et al. Sodium cholate, a solubilizing agent for the necrosis avid radio-iodinated hypericin in rabbits with acute myocardial infarction. *Drug Deliv* 2015;**22**:427–35.

175. Cona MM, Alpizar YA, Li J, Bauwens M, Feng Y, Sun Z, et al. Radioiodinated hypericin: its biodistribution, necrosis avidity and therapeutic efficacy are influenced by formulation. *Pharm Res* 2014;**31**:278–90.

176. Ishikawa M, Hashimoto Y. Improvement in aqueous solubility in small molecule drug discovery programs by disruption of molecular planarity and symmetry. *J Med Chem* 2011;**54**:1539–54.

177. Lewin G, Maciuk A, Moncomble A, Cornard J-P. Enhancement of the water solubility of flavone glycosides by disruption of molecular planarity of the aglycone moiety. *J Nat Prod* 2013;**76**:8–12.

178. Zhang D, Jiang C, Yang S, Gao M, Huang D, Wang X, et al. Effects of skeleton structure on necrosis targeting and clearance properties of radioiodinated dianthrones. *J Drug Target* 2016;**24**:566–77.

179. Feng Y, Chen F, Ma Z, Dekeyzer F, Yu J, Xie Y, et al. Towards stratifying ischemic components by cardiac MRI and multifunctional stainings in a rabbit model of myocardial infarction. *Theranostics* 2013;**4**:24–35.

180. Yao L, Xue X, Yu P, Ni Y, Chen F. Evans blue dye: a revisit of its applications in biomedicine. *Contrast Media Mol Imaging* 2018;**2018**:Article ID 7628037.

181. Jin Q, Shan X, Luo Q, Zhang D, Zhao Y, Yao N, et al. ^{131}I-Evans blue: evaluation of necrosis targeting property and preliminary assessment of the mechanism in animal models. *Acta Pharm Sin B* 2018;**8**:390–400.